Supporting information for:

A Polarizable Force Field of Dipalmitoylphosphatidylcholine based on the Classical Drude Model for Molecular Dynamics Simulations of Lipids

Janamejaya Chowdhary,[†] Edward Harder,[‡] Pedro E. M. Lopes,[¶] Lei Huang,[†]

Alexander D. MacKerell Jr.,[*,¶] and Benoît Roux[*,†]

E-mail: alex@outerbanks.umaryland.edu; roux@uchicago.edu

[*]To whom correspondence should be addressed

[†]Department of Biochemistry and Molecular Biology, Gordon Center for Integrative Science, University of Chicago, Chicago, Illinois, 60637

[‡]Schrödinger Inc., New York, NY 10036

[¶]Department of Pharmaceutical Sciences, School of Pharmacy, University of Maryland Baltimore, Maryland, 21201

1 Electrostatic parameters for model compounds

The optimized electrostatic parameters for methyl acetate, dimethyl phosphate, as well as ammonium, methyl ammonium, dimethyl ammonium, trimethyl ammonium and tetramethyl ammonium cations are presented in Tables S1, S3, S4, S5, S6, S7, and S8. The lone pair definition and anisotropic polarizability for methyl acetate are defined in Table S2.

Table S1: Electrostatic parameters for methyl acetate

Atom Name	Atom Type	Charge	Polarizability	Thole
C1	CD33C	-0.275	-1.993	0.410
C	CD203A	0.697	-1.370	1.747
OM	OD30C	0.000	-0.732	0.601
C2	CD33C	-0.030	-1.797	0.410
O	OD2C3A	0.000	-0.904	0.565
H11	HDA3A	0.069		
H12	HDA3A	0.069		
H13	HDA3A	0.069		
H21	HDA3A	0.116		
H22	HDA3A	0.116		
H23	HDA3A	0.116		
LP1A	LP	-0.349		
LP1B	LP	-0.258		
LPMA	LP	-0.170		
LPMB	LP	-0.170		

Table S2: Lone pair position and anisotropic polarizability for methyl acetate

LONEPAIR relative LP1A O C C1 distance 0.30 angle 91.0 dihe 0.0
LONEPAIR relative LP1B O C C1 distance 0.30 angle 91.0 dihe 180.0
LONEPAIR relative LPMA OM C C2 distance 0.35 angle 110.9 dihe 91.0
LONEPAIR relative LPMB OM C C2 distance 0.35 angle 110.9 dihe 269.0

ANISOTROPY O C LP1A LP1B A11 0.6968 A22 1.2194
ANISOTROPY OM C LPMA LPMB A11 0.8108 A22 1.2162

Table S3: Electrostatic parameters for dimethyl phosphate

Atom Name	Atom Type	Charge	Polarizability	Thole
P	PD1A	1.191	-0.974	2.098
O13	OD2C2B	-0.876	-0.931	1.083
O14	OD2C2B	-0.876	-0.931	1.083
O11	OD30B	-0.470	-0.901	0.181
O12	OD30B	-0.470	-0.901	0.181
C1	CD33C	0.173	-1.642	0.862
H11	HDA3A	0.026		
H12	HDA3A	0.026		
H13	HDA3A	0.026		
C2	CD33C	0.173	-1.642	0.862
H21	HDA3A	0.026		
H22	HDA3A	0.026		
H23	HDA3A	0.026		

Table S4: Electrostatic parameters for ammonium cation

Atom Name	Atom Type	Charge	Polarizability	Thole
N	ND3P3A	-0.692	-1.400	
HN1	HDP1B	0.423		
HN2	HDP1B	0.423		
HN3	HDP1B	0.423		
HN4	HDP1B	0.423		

Table S5: Electrostatic parameters for methyl ammonium cation

Atom Name	Atom Type	Charge	Polarizability	Thole
N	ND3P3A	-0.349	-1.298	0.895
C1	CD33A	-0.100	-1.656	0.895
HN2	HDP1B	0.340		
HN3	HDP1B	0.340		
HN4	HDP1B	0.340		
H11	HDA3C	0.143		
H12	HDA3C	0.143		
H13	HDA3C	0.143		

Table S6: Electrostatic parameters for dimethyl ammonium cation

Atom Name	Atom Type	Charge	Polarizability	Thole
N	ND3P2A	-0.070	-1.479	0.111
C1	CD33A	-0.043	-1.578	1.429
C2	CD33A	-0.043	-1.578	1.429
HN3	HDP1B	0.266		
HN4	HDP1B	0.266		
H11	HDA3C	0.104		
H12	HDA3C	0.104		
H13	HDA3C	0.104		
H21	HDA3C	0.104		
H22	HDA3C	0.104		
H23	HDA3C	0.104		

Table S7: Electrostatic parameters for trimethyl ammonium cation

Atom Name	Atom Type	Charge	Polarizability	Thole
N	ND3P2A	0.219	-0.661	0.803
C1	CD33A	-0.107	-1.527	2.113
C2	CD33A	-0.107	-1.527	2.113
C3	CD33A	-0.107	-1.527	2.113
HN4	HDP1B	0.202		
H11	HDA3C	0.100		
H12	HDA3C	0.100		
H13	HDA3C	0.100		
H21	HDA3C	0.100		
H22	HDA3C	0.100		
H23	HDA3C	0.100		
H31	HDA3C	0.100		
H32	HDA3C	0.100		
H33	HDA3C	0.100		

Table S8: Electrostatic parameters for tetramethyl ammonium cation

Atom Name	Atom Type	Charge	Polarizability	Thole
N	ND3P2A	0.688	-0.829	0.793
C1	CD33A	-0.288	-1.793	1.099
C2	CD33A	-0.288	-1.793	1.099
C3	CD33A	-0.288	-1.793	1.099
C4	CD33A	-0.288	-1.793	1.099
H11	HDA3C	0.122		
H12	HDA3C	0.122		
H13	HDA3C	0.122		
H21	HDA3C	0.122		
H22	HDA3C	0.122		
H23	HDA3C	0.122		
H31	HDA3C	0.122		
H32	HDA3C	0.122		
H33	HDA3C	0.122		
H41	HDA3C	0.122		
H42	HDA3C	0.122		
H43	HDA3C	0.122		

2 Lennard-Jones Parameters

The optimized Lennard-Jones parameters for model compounds are presented in Tables S9, S10 and S11.

Table S9: Lennard-Jones parameters for methyl acetate

Atom type	$E_{min}(kcal/mol)$	$\frac{R_{min}}{2}$ Å
CD33C	-0.078	1.940
CD2O3A	-0.030	1.7750
OD2C3A	-0.180	1.7500
OD30C	-0.122	1.7500

Table S10: Lennard-Jones parameters for dimethyl phosphate

Atom type	$E_{min}(kcal/mol)$	$\frac{R_{min}}{2}$ Å
PD1A	-0.270	1.900
OD2C2B	-0.190	1.970
OD30B	-0.170	1.770
HDA3A	-0.024	1.3400

Table S11: Lennard-Jones parameters for ammonium cations

Atom type	$E_{min}(kcal/mol)$	$\frac{R_{min}}{2}$ Å
ND3P2A	-0.200	1.740
ND3P3A	-0.200	1.740
CD33A	-0.078	2.040
HDP1B	-0.075	0.550
HDA3C	-0.075	0.925

3 NBFIX parameters

Table S12: NBFIX parameters for methyl acetate water interactions.

	E_{min}	R_{min}
CD2O3A-ODW	-0.03235	3.55798
OD2C3A-ODW	-0.27942	3.62321
OD30C-ODW	-0.16583	3.53691

4 DIHEDRAL OPTIMIZATION

The FF and QM energies for the all configurations from relaxed 1-D potential energy scans and rotamers of the residue GLYP are compared in Figure S1.

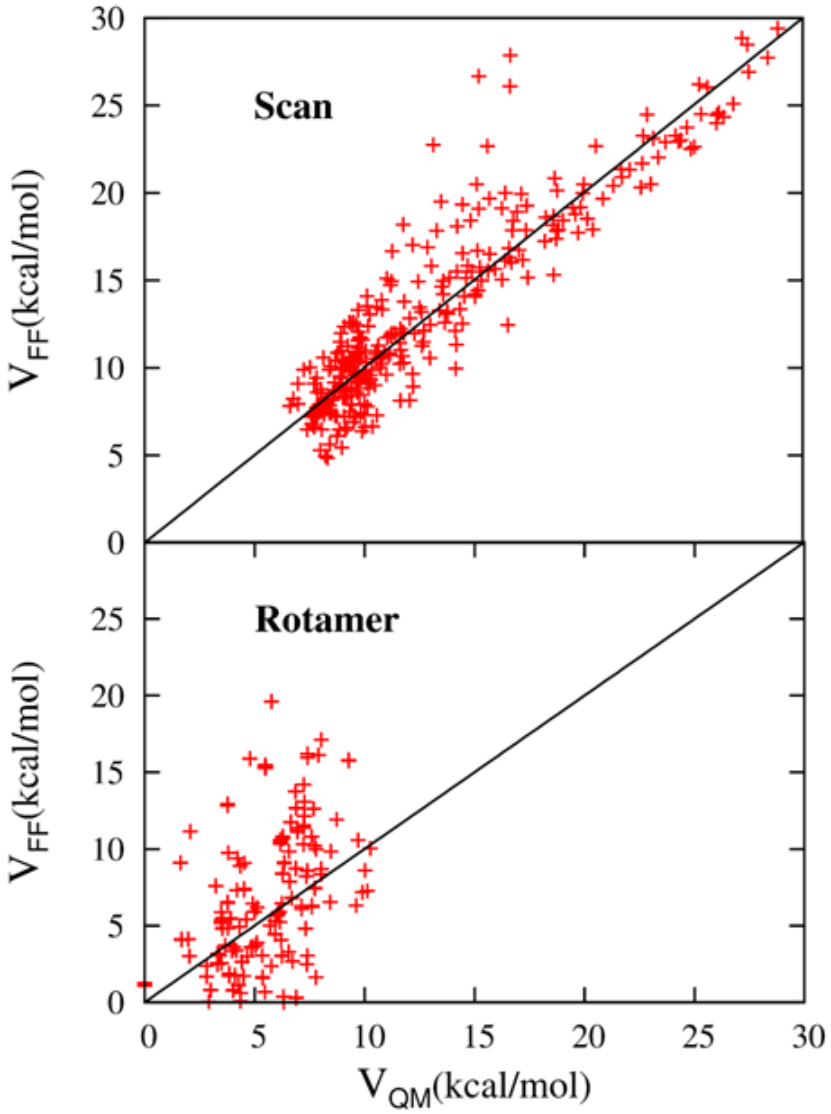

Figure S1: Energy of all configurations obtained from QM (a) relaxed 1-D potential energy scans (top) and (b) rotamers (bottom) compared with the energy of the same configuration, as calculated from the FF. The global energy minimum configuration has zero energy.

5 Thermodynamic properties for small molecules

5.1 Methyl acetate

The stability of the crystal is ascertained by performing a simulation of the crystal with all lattice parameters allowed to fluctuate. The resulting time series of lattice parameters is presented in Figure S2. The thermodynamic properties of models from the grid search with molar volume and enthalpy of vaporization within 5 percentage of the experimental values are presented in Table S13 along with the dielectric constants.

Table S13: Calculated molar volume (V_m), enthalpy of vaporization (H_{vap}), and dielectric constant (ϵ_0 and ϵ_∞) for shortlisted Lennard-Jones models of methyl acetate.

Model	V_m	H_{vap}	ϵ_0	ϵ_∞
1	131.78 ± 6	7.6 ± 0.4	6.9 ± 0.6	1.5 ± 0.2
2	130.28 ± 5	7.66 ± 0.3	6.9 ± 0.5	1.5 ± 0.2
3	130.82 ± 6	7.67 ± 0.4	7 ± 0.5	1.5 ± 0.2
4	131.13 ± 4	7.58 ± 0.4	6.9 ± 0.6	1.5 ± 0.2
5	130.75 ± 7	7.62 ± 0.3	7.1 ± 0.5	1.5 ± 0.2
6	130.92 ± 6	7.62 ± 0.4	6.8 ± 0.6	1.5 ± 0.2
7	130.60 ± 6	7.7 ± 0.3	7.2 ± 0.6	1.5 ± 0.2

5.2 Hydration free energy for ions

All data and calculations are reported for a temperature of 298 K. The experimental gas-phase free energies use as the reference state an ideal gas at 1 atm and the corresponding free energies are identified by the superscript "o". The experimental and computed hydration free energies use for the reference state an ideal gas at a gas-phase concentration of 1 mol/L and an ideal solution at a liquid-phase concentration of 1 mol/L. These free energies will be identified by the superscript "*". The relationship between these two standard states is:

$$\Delta G^{0\to *} = k_{\mathrm{B}} T \ln(24.46) \tag{1}$$

At 298 K, $\Delta G^{0\rightarrow *} = 1.9$ kcal/mol.

The experimental free energy of hydration of dimethylphosphate was obtained from following thermodynamic cycle shown in Figure S3.

Experimental data used includes gas-phase acidity of hydrogen DMP (HDMP) (325Âś4 kcal/mol),[S1] pKa of HDMP 1.29[S2] solvation free energy of H+ (-259.5 kcal/mol) obtained from Drude polarizable force field free energy calculations (-247.0 kcal/mol)[S3] after correcting for the air-water interfacial potential (-12.5 kcal/mol).[S4] The solvation free energy of HDMP was extrapolated using experimental solvation free energies of trimethylphosphate (-8.70 kcal/mol) and solvation FE difference of acetic acid (-6.70 kcal/mol) and methyl acetate (-3.32 kcal/mol) (Sup. Info of reference [S5]). Free energies of hydration for the methyl substituted ammonium cations up to trimethyl substitution were obtained from published values.[S5–S9] Reported hydration free energies for the same ion often differ depending on the experimental source. To account for this inconsistency, the experimental data is adjusted such that the reported experimental data of the proton (-264 kcal/mol)[S10] is consistent with that of a recent parametrization for the Drude model (-259.5 kcal/mol). An experimental estimate of the free energy of hydration of tetramethylphosphate was given by Boyd based on the lattice energy of tetramethylammonium halides.[S11]

The calculated free energy of hydration for dimethyl phosphate and ammonium cations are presented in Table S14. For each ion, the average of 7 independent calculations as well as entropic and boundary potential corrections are included. LRC are set at -1.0 kcal/mol.

Table S14: Experimental and calculated free energies of hydration (kcal/mol) of dimethyl phosphate and ammonium cations

Ion	Experiment	Drude
DMP-	-78 ± 4	-79 ± 0.2
Ammonium	-78 ± 3	-79.8 ± 0.2
Methylammonium	-69 ± 3	-69.5 ± 0.2*
Dimethylammonium	-62 ± 2	-61.6 ± 0.2*
Trimethylammonium	-55 ± 1	-55.9 ± 0.2*
Tetramethylammonium	-45	-51.8 ± 0.3*

6 Bilayer properties

6.1 Area per lipid from long trajectory

The area per lipid from three 150 ns simulations are presented in Figure S4. The bilayer stabilizes to an average area of 60Å^2 and does not undergo a gel transition.

6.2 Distribution of Dihedral angles

Since the order parameters, shown in the main text, for the Drude model differ from experiments and the C36 FF primarily for the G3, G2, and G1 positions, the distribution of dihedral angles for the associated dihedrals should provide insight into the reasons behind these differences. In Figure S5, we define the position of DPPC atoms for which dihedral angle distributions will be presented. The probability distribution functions for the P-O_{11}-G_3-G_2, O_{11}-G_3-G_2-G_1, G_3-G_2-G_1-O_{31}, G_3-G_2-O_{21}-C_{21} and G_2-G_1-O_{31}-C_{31} dihedral angles are presented in the following figures. There are clear differences between the Drude and C36 FFs. The distribution for P-O_{11}-G_3-G_2 shows the biggest deviation from C36. It should be noted that the 1-D relaxed potential energy scan for the dihedral angle (α_1 in Figure 5 of main text) from the FF does not reproduce the low energy part of the scan although it does get the overall shape reasonably well. Given that C36 gives good agreement for the deuterium order parameters, subsequent improvement of the Drude FF will focus on improving the parameters for torsions which show the most deviation from C36, particularly the low energy part of the torsion energy surface.

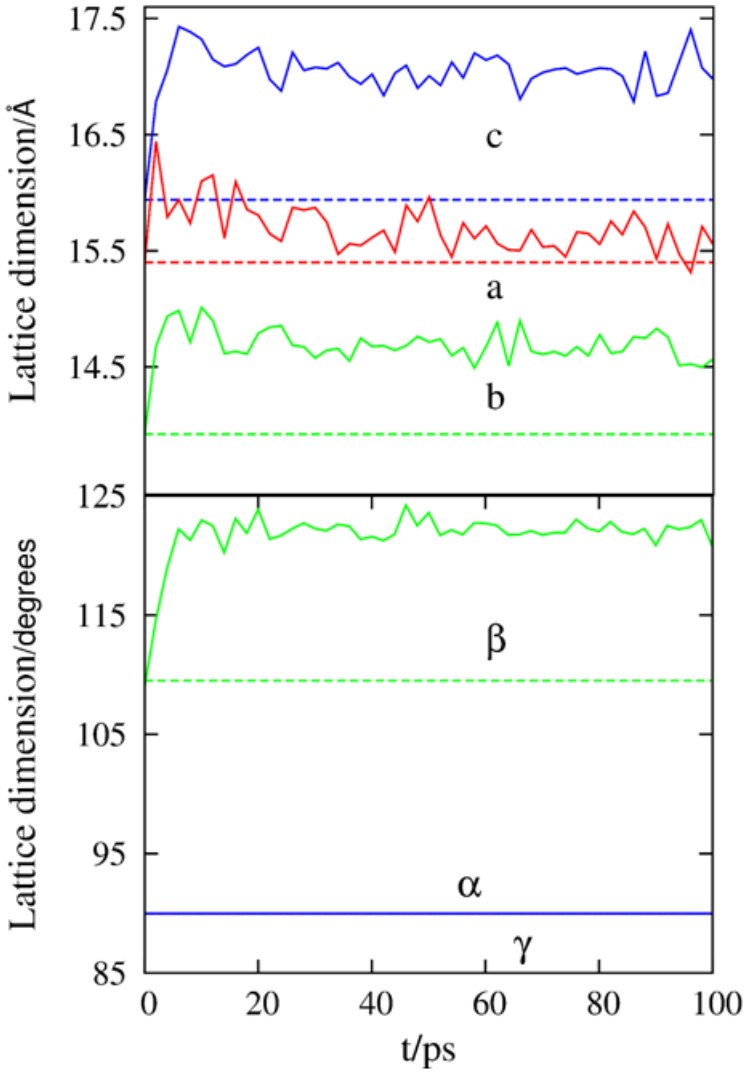

Figure S2: The time variation of lattice parameters (a,b,c,α,β and γ) for the Methyl Acetate crystal from a 100 ps simulation at a temperature of 145K. The deviation from the crystal lattice are within 10

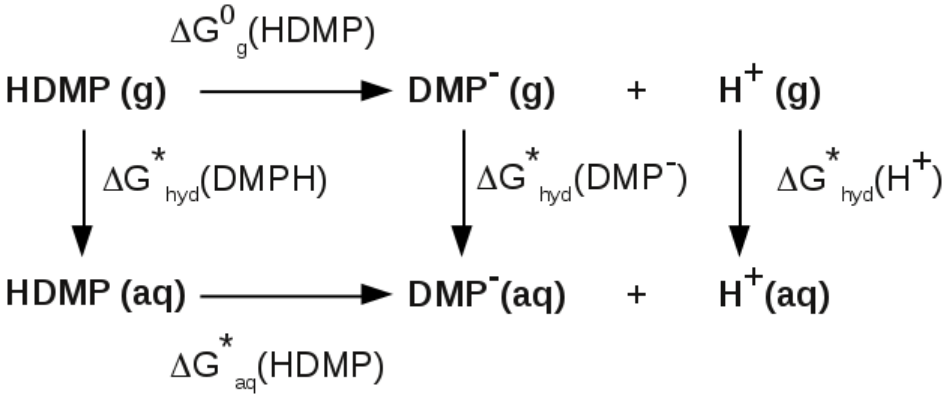

Figure S3: Thermodynamic cycle used to determine the hydration free energy of dimethyl phosphate anion

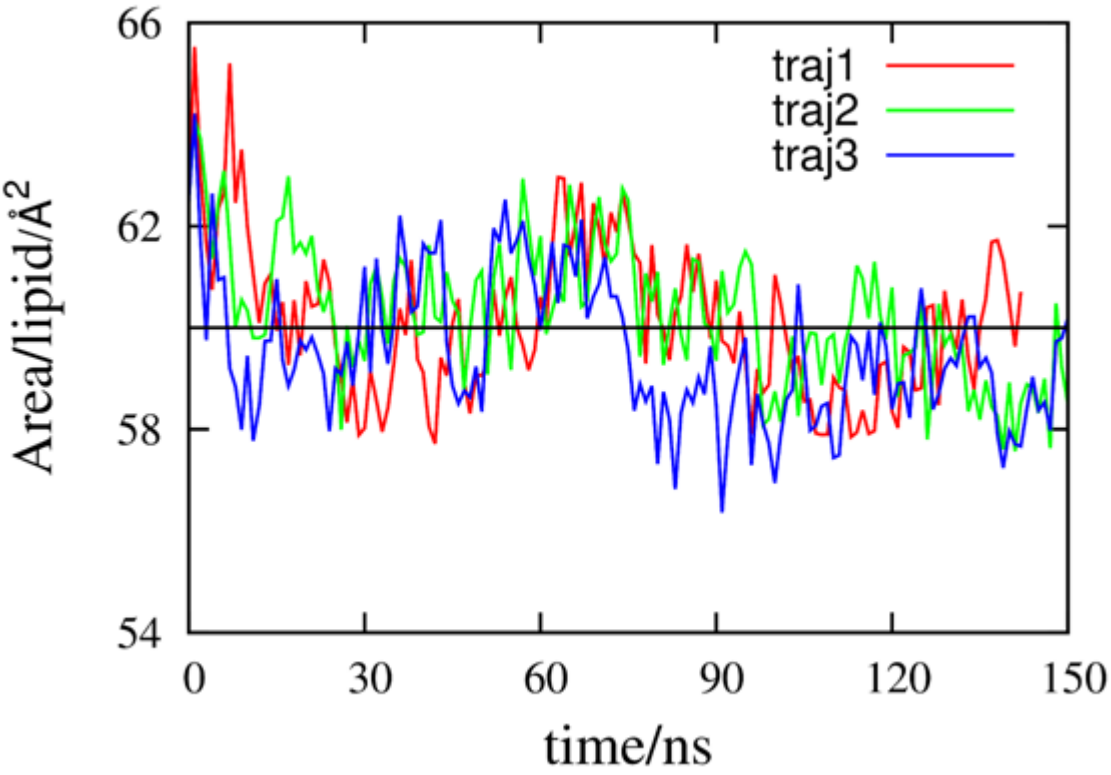

Figure S4: Area per lipid from three simulations (traj1, traj2, traj3) of the DPPC bilayer starting with the same configuration but different velocities. The system is stable for the entire duration of the simulation and the average area per lipid is 60 Å^2.

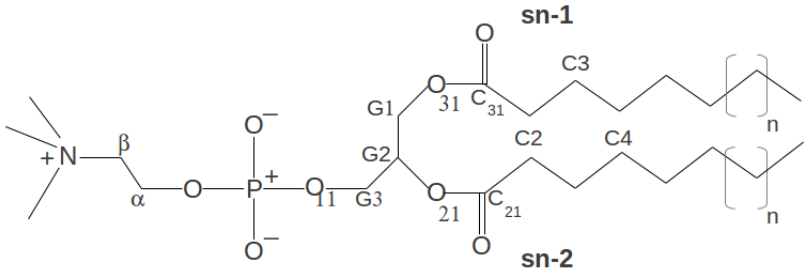

Figure S5: Nomenclature of the atoms used for constructing the distribution of dihedral angles for the DPPC molecule

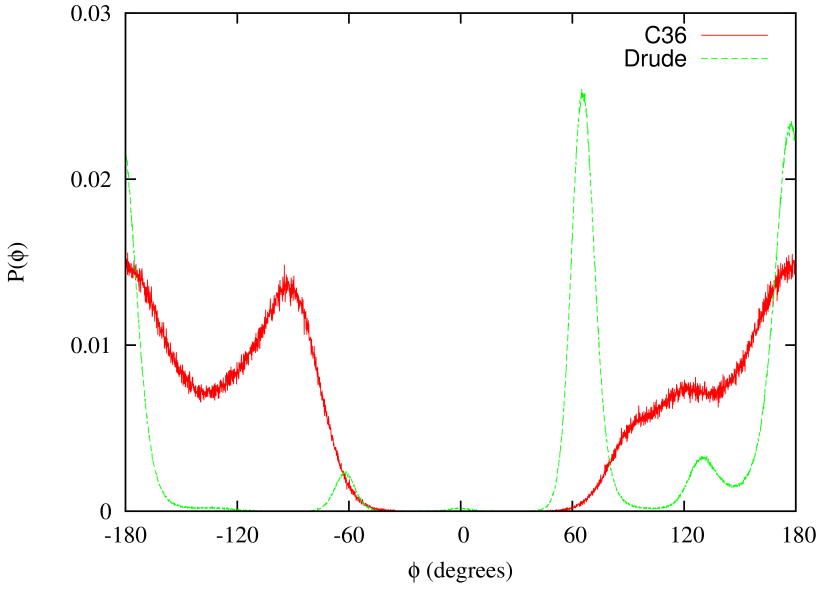

Figure S6: Distribution of dihedral angles for the P-O_{11}-G_3-G_2 torsion

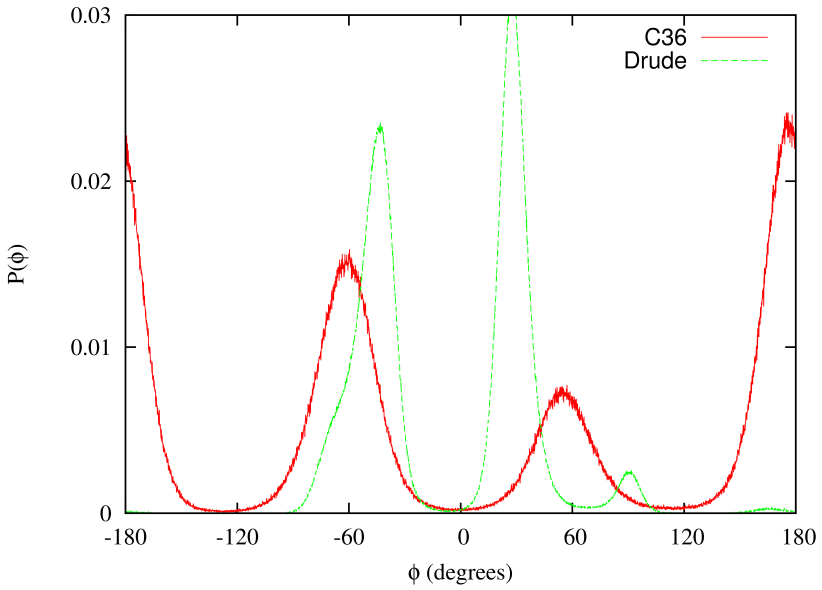

Figure S7: Distribution of dihedral angles for the O_{11}-G_3-G_2-G_1 torsion

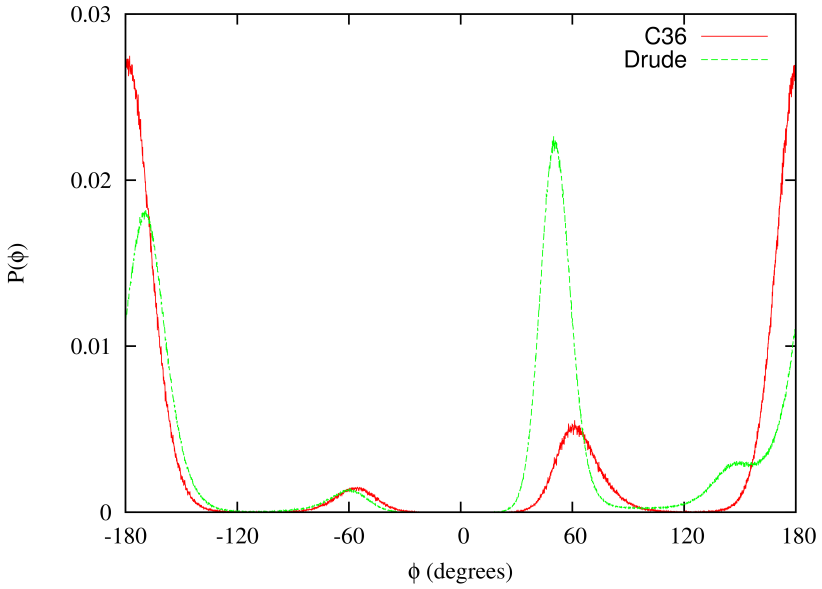

Figure S8: Distribution of dihedral angles for the G_3-G_2-G_1-O_{31} torsion

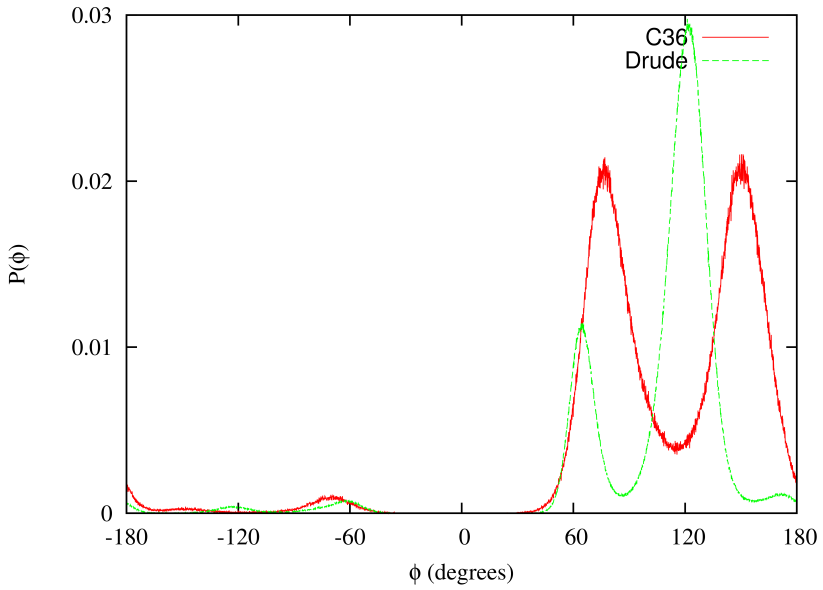

Figure S9: Distribution of dihedral angles for the G_3-G_2-O_{21}-C_{21} torsion

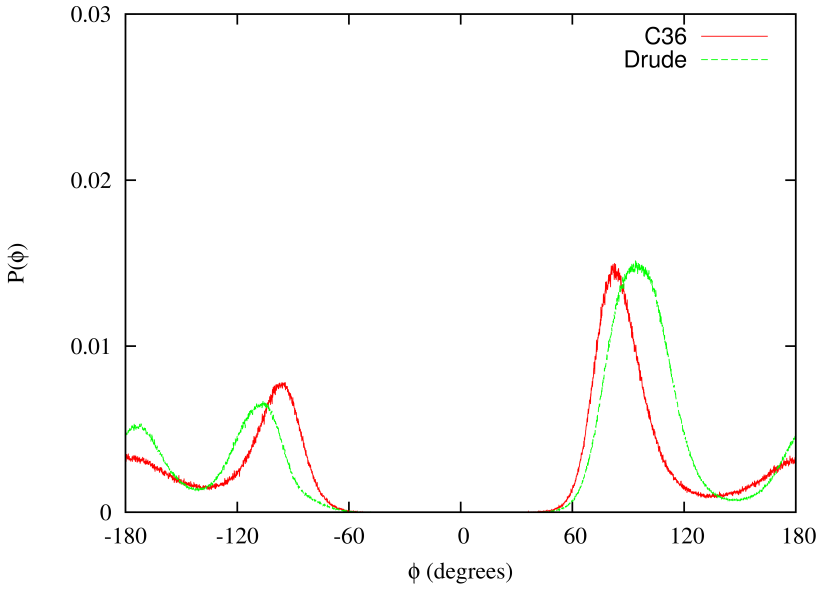

Figure S10: Distribution of dihedral angles for the G_2-C_1-O_{31}-C_{31} torsion

References

(S1) Lum, R. C.; Grabowski, J. J. Trimethyl phosphate: the intrinsic reactivity of carbon versus phosphorus sites with anionic nucleophiles. *J. Am. Chem. Soc.* **1992**, *114*, 8619–8627.

(S2) Lopez, X.; Schaefer, M.; Dejaegere, A.; Karplus, M. Theoretical Evaluation of pKa in Phosphoranes: Implications for Phosphate Ester Hydrolysis. *J. Am. Chem. Soc.* **2002**, *124*, 5010–5018.

(S3) Lamoureux, G.; Roux, B. Absolute hydration free energy scale for alkali and halide ions established from simulations with a polarizable force field. *J. Phys. Chem. B* **2006**, *110*, 3308–3322.

(S4) Lamoureux, G.; MacKerell, A. D.; Roux, B. A simple polarizable model of water based on classical Drude oscillators. *J. Chem. Phys.* **2003**, *119*, 5185–5197.

(S5) Kelly, C. P.; Cramer, C. J.; Truhlar, D. G. SM6: A density functional theory continuum solvation model for calculating aqueous solvation free energies of neutrals, ions, and solute-water clusters. *J. Chem. Theory Comput.* **2005**, *1*, 1133–1152.

(S6) Pearson, R. G. Ionization potentials and electron affinities in aqueous solution. *J. Am. Chem. Soc.* **1986**, *108*, 6109–6114.

(S7) Florian, J.; Warshel, A. Langevin dipoles model for ab initio calculations of chemical processes in solution: Parametrization and application to hydration free energies of neutral and ionic solutes and conformational analysis in aqueous solution. *J. Phys. Chem. B* **1997**, *101*, 5583–5595.

(S8) Pliego, J. R.; Riveros, J. M. Gibbs energy of solvation of organic ions in aqueous and dimethyl sulfoxide solutions. *Phys. Chem. Chem. Phys.* **2002**, *4*, 1622–1627.

(S9) Kelly, C. P.; Cramer, C. J.; Truhlar, D. G. Aqueous solvation free energies of ions and ionâĹŠwater clusters based on an accurate value for the absolute aqueous solvation free energy of the proton. *J. Phys. Chem. B* **2006**, *110*, 16066–16081.

(S10) Tissandier, M. D.; Cowen, K. A.; Feng, W. Y.; Gundlach, E.; Cohen, M. H.; Earhart, A. D.; Coe, J. V.; T. R. Tuttle, J. The proton's absolute aqueous enthalpy and Gibbs free energy of solvation from cluster-ion solvation data. *J. Phys. Chem. A* **1998**, *102*, 7787–7794.

(S11) Boyd, R. H. Lattice Energies and Hydration Thermodynamics of Tetra-alkylammonium Halides. *J. Chem. Phys.* **1969**, *51*, 1470–1474.